NANO EXPRESS   **Open Access**

CdS Nanoparticle-Modified α-Fe$_2$O$_3$/TiO$_2$ Nanorod Array Photoanode for Efficient Photoelectrochemical Water Oxidation

Ruiyang Yin[1], Mingyang Liu[1], Rui Tang[2] and Longwei Yin[2*]

Abstract

In this work, we demonstrate a facile successive ionic layer adsorption and reaction process accompanied by hydrothermal method to synthesize CdS nanoparticle-modified α-Fe$_2$O$_3$/TiO$_2$ nanorod array for efficient photoelectrochemical (PEC) water oxidation. By integrating CdS/α-Fe$_2$O$_3$/TiO$_2$ ternary system, light absorption ability of the photoanode can be effectively improved with an obviously broadened optical-response to visible light region, greatly facilitates the separation of photogenerated carriers, giving rise to the enhancement of PEC water oxidation performance. Importantly, for the designed abnormal type-II heterostructure between Fe$_2$O$_3$/TiO$_2$, the conduction band position of Fe$_2$O$_3$ is higher than that of TiO$_2$, the photogenerated electrons from Fe$_2$O$_3$ will rapidly recombine with the photogenerated holes from TiO$_2$, thus leads to an efficient separation of photogenerated electrons from Fe$_2$O$_3$/holes from TiO$_2$ at the Fe$_2$O$_3$/TiO$_2$ interface, greatly improving the separation efficiency of photogenerated holes within Fe$_2$O$_3$ and enhances the photogenerated electron injection efficiency in TiO$_2$. Working as the photoanodes of PEC water oxidation, CdS/α-Fe$_2$O$_3$/TiO$_2$ heterostucture electrode exhibits improved photocurrent density of 0.62 mA cm^{-2} at 1.23 V vs. reversible hydrogen electrode (RHE) in alkaline electrolyte, with an obviously negatively shifted onset potential of 80 mV. This work provides promising methods to enhance the PEC water oxidation performance of the TiO$_2$-based heterostructure photoanodes.

Keywords: TiO$_2$, α-Fe$_2$O$_3$, CdS, Nanorod, Photoelectrochemical Water Oxidation

Background

To solve the severe problem of pollution and limited resources of fossil, photoelectrochemical (PEC) water splitting to produce hydrogen has been regarded as one of the most promising strategies for solar energy conversion. Since the first report on PEC water oxidation based on TiO$_2$ [1], TiO$_2$ has drawn much attention as the photoanode materials for PEC water oxidation, due to its stable PEC properties, strong optical response, and suitable energy band position [2, 3]. However, the PEC performance of pristine TiO$_2$ photoanode is greatly confined by the slow water oxidation kinetics originated from the poor photogenerated carrier separation capability and insufficient light absorption ability [4, 5].

Therefore, various strategies have been taken to improve the PEC water oxidation performance of pristine TiO$_2$, such as surface modification [6], quantum dot sensitization, and heterojunction construction [7, 8]. One efficient method to improve the photogenerated carrier separation performance is to construct heterostructured photoanode. For instance, constructing heterojunction between TiO$_2$ and other metal oxide semiconductors with matched energy band structures (like Co$_3$O$_4$/TiO$_2$ [9] and ZnIn$_2$S$_4$/TiO$_2$ [10, 11]) can effectively facilitate the separation of photogenerated electrons and holes; therefore, PEC water splitting performance of the pristine TiO$_2$ can be obviously enhanced. Among various metal oxide semiconductors, hematite (α-Fe$_2$O$_3$) is regarded as a promising photoanode material because of the suitable band gap (~ 2.0 eV) for sunlight harvesting, excellent stability, and low cost [12]. In addition, the theoretical power conversion efficiency (PCE) of α-Fe$_2$O$_3$ can reach 15.3%, with a photocurrent density of 12.6 mA cm^{-2} at 1.23 V vs. reversible hydrogen electrode (RHE) under the

* Correspondence: yinlw@sdu.edu.cn
[2]Key Laboratory for Liquid–Solid Structural Evolution and Processing of Materials, Ministry of Education, School of Materials Science and Engineering, Shandong University, Jinan 250061, People's Republic of China
Full list of author information is available at the end of the article

Yin *et al. Nanoscale Research Letters* (2017) 12:520

Page 2 of 8

standard sun irradiation [13]. Therefore, constructing α-Fe_2O_3/TiO_2 heterostructured photoanode cannot only enhance the carrier separation performance in TiO_2 but also effectively extend the light absorption range of TiO_2. Meanwhile, according to some latest research, α-Fe_2O_3 photoanodes suffer from short electron-hole pair lifetime and hole diffusion length (2–4 nm), which results in high recombination rate of photogenerated carriers, hindering the improvement of the PEC performance [12]. In that case, to further enhance the PEC water splitting performance of Fe_2O_3/TiO_2 photoanodes, some narrow band gap semiconductors, like CdS [14, 15] and PbS [16], can be coupled to facilitate the separation of photogenerated carriers. Among them, $CdS/Fe_2O_3/TiO_2$ heterostructured photoanode is considered to be a promising choice with matched band gap and expanded light absorption range. Also, carrier transport process can be effectively improved because photogenerated carriers can be quickly separated at the interface of $CdS/Fe_2O_3/TiO_2$, thereby greatly decreasing the carrier recombination rates.

What is more, in order to construct an advanced electrode for PEC water splitting system, the electrode materials should possess the characteristics like sufficient incident light capture capability and tunnels for charge transport. Comparing with general planar photoanodes, one dimensional (1D) nanorod (NR) array photoanodes exhibit good incident light harvesting performance due to the enhanced multi-scattering processes [17], which would lead to an enhanced PEC water oxidation performance. Besides, it is reported that 1D NR array also exhibits excellent carrier transport performance since the photogenerated carriers can directly transport along the NR, thus direct carrier recombination at the crystal boundary can be effectively avoided [18]. Also, in order to further enlarge the surface area of such 1D NR arrays, which can bring more PEC reaction sites and enhance the PEC performance, 1D NR with branched nanostructures is expected [19]. Such integrated architecture offers a long optical path for effective light harvesting, short diffusion distance for excellent charge transport, and large surface area for fast interfacial charge collection, which is of great benefit for the enhancement of PEC performance. Hence, it would be of particular interest to design a CdS-modified Fe_2O_3/TiO_2 heterostructure NR array for PEC water oxidation.

Herein, we reported a facile successive ionic layer adsorption and reaction (SILAR)-hydrothermal method to synthesize CdS-modified Fe_2O_3/TiO_2 NR array for efficient PEC water oxidation. UV-vis study confirms the $CdS/Fe_2O_3/TiO_2$ NR array displays excellent optical response performance with an obvious broadened light absorption range. Improved charge transfer process and declined charge recombination rate can be evidenced by means of PL spectrum and EIS plots. Applied as the photoanode for PEC water oxidation, $CdS/Fe_2O_3/TiO_2$ NR array exhibits greatly enhanced photocurrent density of 0.62 mA cm^{-2} (1.23 V vs. RHE) in alkaline electrolyte compared with pristine TiO_2 (0.32 mA cm^{-2} at 1.23 V vs. RHE). It is believed that the synthesis route and the application of $CdS/Fe_2O_3/TiO_2$ NR array presently reported is of great importance and can be applied in other photovoltaic and photoelectronic devices.

Methods

Preparation of CdS/Fe$_2$O$_3$/TiO$_2$ NR Heterostructured Photoanode

Synthesis of TiO$_2$ NR Array

To synthesize TiO_2 NR array on the FTO glass, the FTO was cut into rectangle and ultrasonically cleaned with deionized water, acetone, and ethanol, successively. Then, the FTO was put into the autoclave containing a mixed solution of deionized water (20 ml), hydrochloric acid (20 ml), and titanium isopropoxide (1.1 ml) and baked at 160 °C for 6 h. After the reaction, the FTO was washed with deionized water and ethanol for several times and then was annealed in air at 450 °C for 0.5 h.

Synthesis of Fe$_2$O$_3$/TiO$_2$ NR Array

To grow α-Fe_2O_3 on TiO_2 NR, as obtained TiO_2 NR array was put into a mixed solution of $FeCl_3$ (15 ml, 0.1 M) and $NaNO_3$ (15 ml, 0.5 M) and then transferred to the autoclave. Heating at 100 °C for 2 h, the autoclave was cooled to room temperature and the FTO substrate was washed with deionized water and ethanol for several times. Finally, the FTO substrate was annealed in air at 450 °C for 1 h.

Synthesis of CdS/Fe$_2$O$_3$/TiO$_2$ NR

The obtained α-Fe_2O_3/TiO_2 NR array was pretreated with an ethanol solution of mercaptopropinioc acid (MPA, 0.3 M) overnight at 50 °C and then washed with ethanol to remove the excess MPA. In order to deposit CdS layer, a facile successive ionic layer adsorption and reaction (SILAR) method is applied. Pretreated NR array was successively immersed into four different solutions for 30 s, including $Cd(NO_3)_2 \cdot 4H_2O$ (ethanol, 0.1 M), pure ethanol, $Na_2S \cdot 9H_2O$ (methanol, 0.2 M) and pure methanol, respectively. The SILAR process was repeated for five times and then the substrate was washed with methanol to remove the extra CdS.

Materials Characterization

The phase structures were characterized by X-ray powder diffractometer (XRD) in a 2θ range of 20 to 80°. The morphology of the products was studied with field emission scanning electron microscopy (FE-SEM) attached energy-dispersive X-ray spectroscopy (EDS). Transmission electron microscopy (TEM) images were collected

Yin *et al. Nanoscale Research Letters* (2017) 12:520

Page 3 of 8

via Tecnai 20 U-Twin equipment. The absorption and photoluminescence (PL) spectra were tested with TU-1900 and Hitachi U-4100, respectively.

Photoelectrochemical Performance Characterization

The PEC water oxidation performance was characterized with CHI660E electrochemical station with a three-electrode mode. The applied electrolyte was consisted of 1M NaOH. Before testing, the system was bubbled with argon for 30 min to remove the electrolyte dissolved gas. The linear sweep voltammograms (LSV) and chronoamperometric I-t curves were recorded under standard sunlight illuminations (100 mW cm^{-2}). Mott-Schottky plots were measured in the dark at an AC frequency of 1.0 kHz.

Hereafter, the electrode potential was converted into the RHE potential with the Nernst equation:

$$E_{\text{RHE}} = E_{\text{Ag/AgCl}} + 0.059\,\text{pH} + E^{o}{}_{\text{Ag/AgCl}} \tag{1}$$

where E_{RHE} was the converted potential vs. RHE, $E_{\text{Ag/AgCl}}$ was the measured potential vs. the Ag/AgCl electrode, and $E^{o}_{\text{Ag/AgCl}}$ = 0.1976 V at 25 °C.

Result and Discussion

Structure and Morphology Characterization

The phase structures of the synthesized products are characterized by the XRD patterns in Fig. 1. As shown in Fig. 1a, the rutile TiO$_2$ nanorod arrays (NR) are successfully synthesized. The diffraction peaks at 36.0°, 44.1°, 54.3°, 62.7°, 64.0°, 65.4°, and 69.8° correspond well to (101), (210), (211), (002), (310), (221), and (112) planes of rutile TiO$_2$ (JCPDS. 21-1276). After deposition

of Fe$_2$O$_3$, the additional XRD diffraction peaks at 32.9° and 45.2° can be indexed to (222) and (332) planes of Fe$_2$O$_3$ (JCPDS. 39-0238). SILAR process is applied to grow CdS nanoparticles, the diffraction peaks at 26.4°, 28.2° corresponding well to (002) and (101) planes of CdS (JCPDS. 65-3414) confirm the success growth of CdS nanoparticles on Fe$_2$O$_3$/TiO$_2$. The SEM image in Fig. 1b shows that TiO$_2$ NRs are uniformly grown on the FTO substrate with a diameter of 50 nm. The NR surface is relatively smooth. After growth of Fe$_2$O$_3$ on surface of TiO$_2$, the diameter of Fe$_2$O$_3$/TiO$_2$ gests larger and increases to 60 nm. Furthermore, the surface of the NRs gets much rougher. Further deposition of CdS nanoparticles can cause an increase in diameter of the Fe$_2$O$_3$/TiO$_2$ composite NR. To further confirm element distribution of the obtained CdS/Fe$_2$O$_3$/TiO$_2$ NR, the cross-view EDS mapping images are recorded and shown in Additional file 1: Figure S1, Additional file 2: Figure S2. It can be seen that Ti, Fe, Cd, and S elements are uniformly distributed among samples.

The HRTEM image and selected area electron diffraction (SAED) pattern of CdS/Fe$_2$O$_3$/TiO$_2$ NR are shown in Fig. 2. It can be seen that the both TiO$_2$ and Fe$_2$O$_3$ are well crystallized and the CdS nanoparticles are grown on surface of Fe$_2$O$_3$. The lattice spacing of 0.31, 0.27, and 0.21 nm can be corresponded well to the (101), (222), and (210) plane of CdS, Fe$_2$O$_3$, and TiO$_2$, respectively (Fig. 2a). The diffraction rings from the recorded SAED pattern in Fig. 2b can be seen, which can be indexed well to (101), (210) planes of rutile TiO$_2$, (222), (332) planes of Fe$_2$O$_3$, and (002), (101) planes of CdS, respectively. The TEM results are in good agreement with the XRD characterization results.
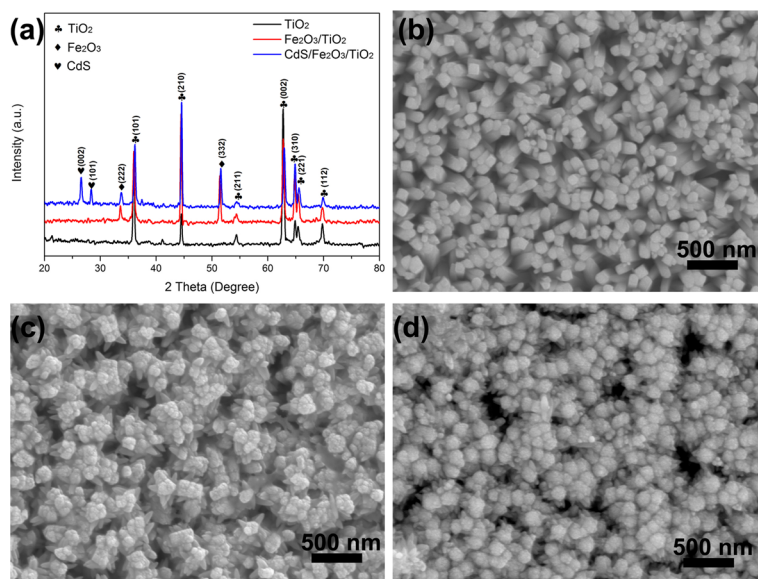

Fig. 1 **a** The XRD patterns and **b** SEM images of TiO$_2$ NR, Fe$_2$O$_3$/TiO$_2$ NR, and CdS/Fe$_2$O$_3$
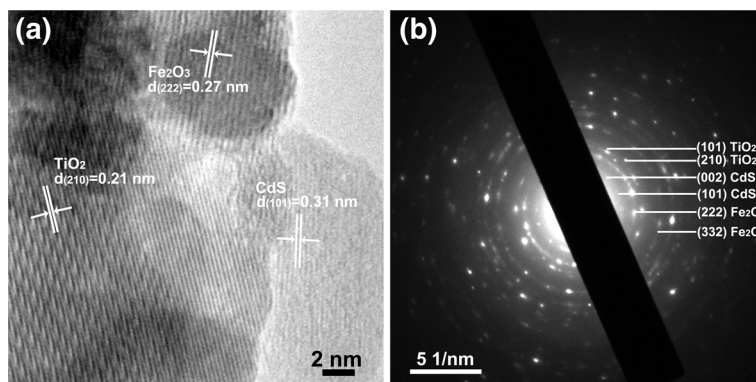
Fig. 2 a HRTEM image of CdS/Fe$_2$O$_3$/TiO$_2$ NR. The marked d-spacing of 0.31 nm corresponds well to the (101) plane of CdS, the d-spacing of 0.27 nm correspond well to the (222) plane of Fe$_2$O$_3$ and the d-spacing of 0.21 nm correspond well to the (210) plane of TiO$_2$. **b** Selected area electron diffraction pattern of CdS/Fe$_2$O$_3$/TiO$_2$ NR, the diffraction rings correspond to the (002), (101) planes of CdS, (222), (332) planes of Fe$_2$O$_3$ and (101), (210) planes of TiO$_2$

The chemical composition and valence states of the CdS/Fe$_2$O$_3$/TiO$_2$ hybrid NRs are studied by XPS spectra. Figure 3a shows the survey spectra, the existence of Ti, Fe, O, Cd, and S elements are demonstrated. The appearance of element C is assigned to the carbon-based containment. For the Ti 2p XPS spectrum in Fig. 3b, these splitted two distinct peaks at 458.2 and 464.2 eV can be assigned to Ti 2 p$_{3/2}$ and 2 p$_{1/2}$ of TiO$_2$ [20]. The XPS spectrum of Fe 2p is shown in Fig. 3c. Two distinct peaks at 710.6 and 724.10 eV can be seen, which correspond well to Fe 2 p$_{3/2}$ and 2 p$_{1/2}$ peaks of α-Fe$_2$O$_3$ [21].

The core level XPS spectrum of O 1s is shown in Fig. 3d, where the peak at 531.2 eV is attributed to the Ti–O bond between titanium and oxygen, and the peak at 531.9 eV can be attributed to the Fe–O bond between iron and oxygen [20, 21]. Figure 3e shows XPS spectrum of Cd, which is attributed to the Cd 3d$_{5/2}$ at 405.2 eV. The XPS spectrum of S 2P is shown in Fig. 3f [22]. The center peak is splitted into two peaks of S 2p$_{1/2}$ and 2p$_{3/2}$ at 161.5 and 162.6 eV [22].

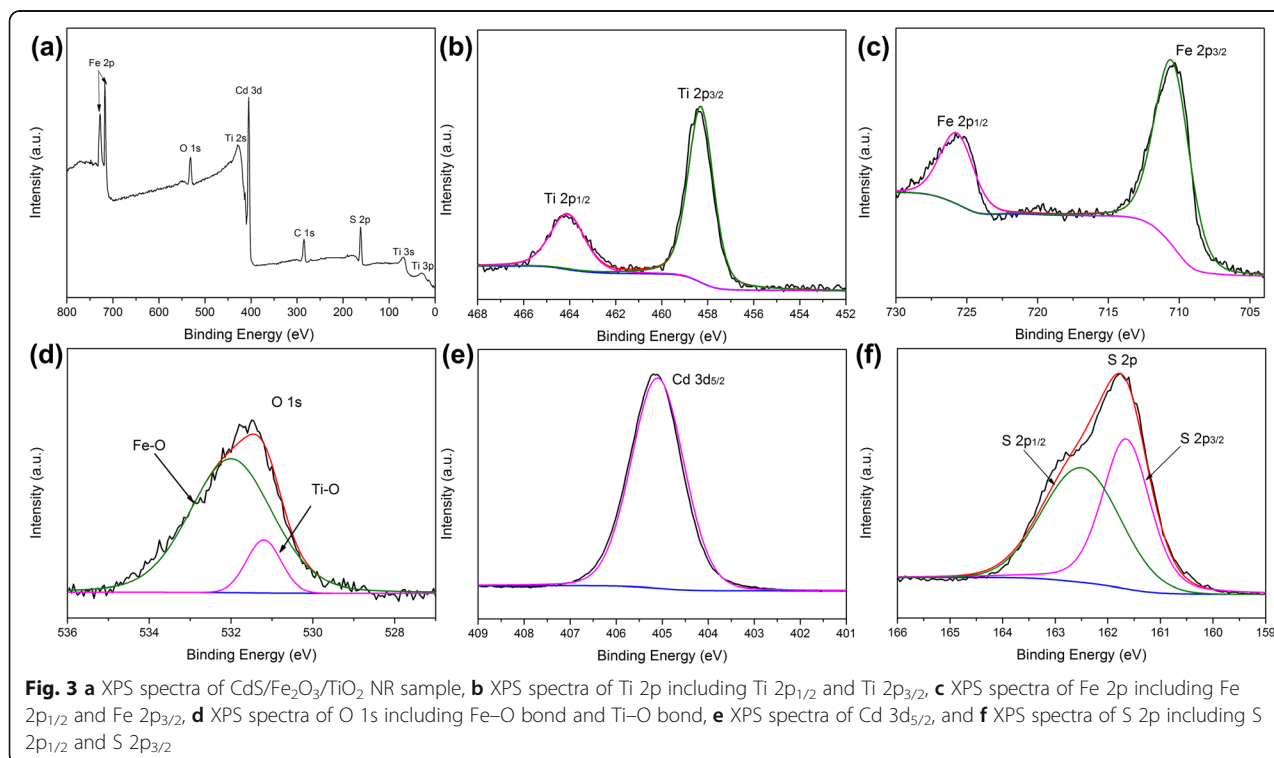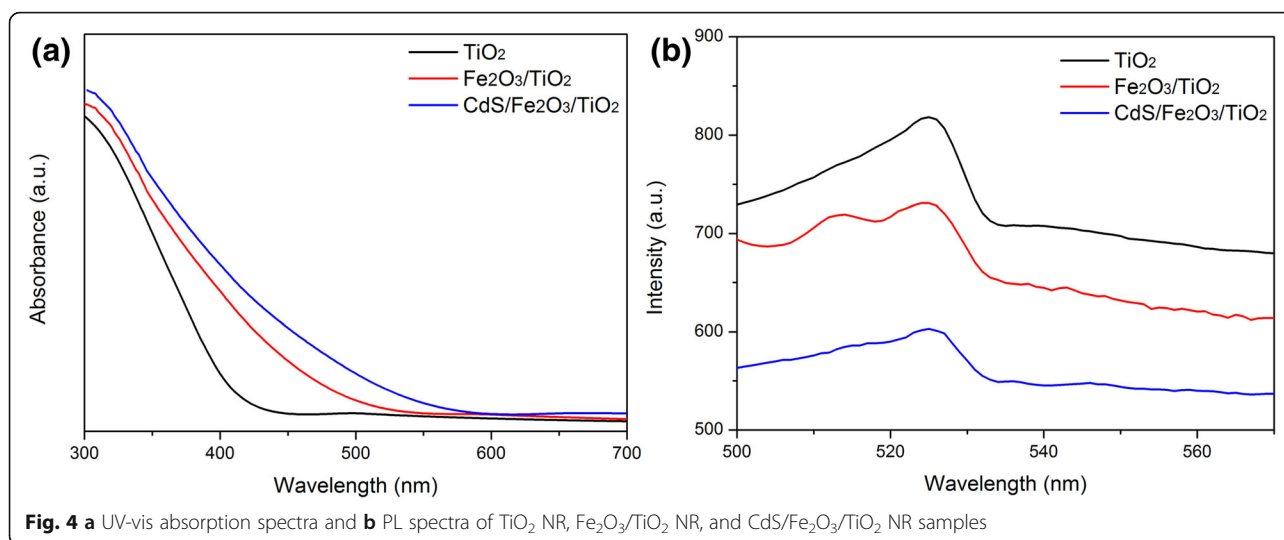Figure 4a shows the absorption spectra of different photoelectrodes. TiO$_2$ shows a typical absorption band

Fig. 3 a XPS spectra of CdS/Fe$_2$O$_3$/TiO$_2$ NR sample, **b** XPS spectra of Ti 2p including Ti 2p$_{1/2}$ and Ti 2p$_{3/2}$, **c** XPS spectra of Fe 2p including Fe 2p$_{1/2}$ and Fe 2p$_{3/2}$, **d** XPS spectra of O 1s including Fe–O bond and Ti–O bond, **e** XPS spectra of Cd 3d$_{5/2}$, and **f** XPS spectra of S 2p including S 2p$_{1/2}$ and S 2p$_{3/2}$
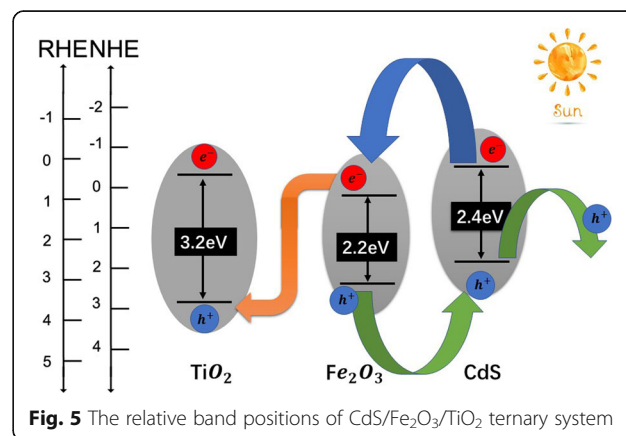
Yin *et al. Nanoscale Research Letters* (2017) 12:520

Page 5 of 8

Fig. 4 a UV-vis absorption spectra and **b** PL spectra of TiO_2 NR, Fe_2O_3/TiO_2 NR, and $CdS/Fe_2O_3/TiO_2$ NR samples

edge at 400 nm, which can be attributed to the intrinsic band gap absorption of TiO_2 (3.2 eV). After coupling with Fe_2O_3, Fe_2O_3/TiO_2 shows enhanced absorption in the visible light region at about 540 nm. The extension of absorption band edge is due to the visible-sensitive component of Fe_2O_3 (2.0–2.2 eV). After further modification of CdS nanoparticles, the light absorption edge can be further extended to 580 nm. It confirms that coupling TiO_2 with Fe_2O_3 and CdS can effectively tune the light absorption property to visible light region. Photoluminescence (PL) spectrum is applied to study the influence of incorporation of CdS and Fe_2O_3 in the $CdS/Fe_2O_3/TiO_2$ hybrid on photogenerated carriers' transport and recombination behavior. The lower the intensity of PL peak, the higher separation efficiency of photogenerated carrier pairs in the samples. Figure 4b shows the PL spectra of TiO_2, Fe_2O_3/TiO_2, and $CdS/Fe_2O_3/TiO_2$ samples. It is obvious that Fe_2O_3/TiO_2 NR achieves lower carrier recombination rate than pristine TiO_2, and $CdS/Fe_2O_3/TiO_2$ NR achieves the best carrier transport performance.

In order to further confirm this conclusion, the picosecond-resolved fluorescence transient plots are tested and shown as Additional file 3: Figure S3. The average lifetime τ is calculated according to $\tau = (B_1\tau_1 [2] + B_2\tau_2 [2])/(B_1\tau_1 + B_2\tau_2)$ and the time constant of the fluorescence transients at 511 nm is listed in the Additional file 4: Table S1 [23]. It can be seen that after modifying pristine TiO_2 with Fe_2O_3, the photogenerated carrier lifetime is prolonged. Coupled with CdS, the carrier lifetime can be further enhanced. This result obviously demonstrates the charge separation performance can be effectively enhanced by forming $CdS/Fe_2O_3/TiO_2$ multi-junction.

The possible carrier transport process is illustrated in Fig. 5. In the $CdS/Fe_2O_3/TiO_2$ ternary system, because both the conduction band position and valence band

position of CdS are higher than that of Fe_2O_3, the photoinduced electrons in CdS will be transported to conduction band of Fe_2O_3, while the photoinduced holes in valence band in Fe_2O_3 will be transported to CdS. For the designed abnormal type-II heterostructure between Fe_2O_3/TiO_2, the conduction band position of Fe_2O_3 is higher than that of TiO_2. Under sunlight illumination, photoexcited electron-hole pairs will generate both in TiO_2 and Fe_2O_3. Photogenerated electrons in the conduction band of Fe_2O_3 will immediately move to the valence band of TiO_2 to recombine with the photogenerated holes, thus greatly improving the separation efficiency of photogenerated holes within Fe_2O_3 and enhances the photogenerated electron injection efficiency in TiO_2 [24, 25]. It implies that the coupling of TiO_2 with Fe_2O_3 and CdS can effectively reduce the recombination rate of the photogenerated carrier pairs. Meanwhile, the photogenerated electrons in TiO_2 move to the counter electrode where the reduction reaction takes place. So, the abnormal type-II heterostructure

Fig. 5 The relative band positions of $CdS/Fe_2O_3/TiO_2$ ternary system

Yin *et al. Nanoscale Research Letters* (2017) 12:520

Page 6 of 8

between Fe_2O_3/TiO_2 plays an important role in the enhanced PEC water oxidation performance.

Figure 6 depicts linear sweep voltammograms (LSV) and chronoamperometric I-*t* curves of $CdS/Fe_2O_3/TiO_2$, Fe_2O_3/TiO_2, and TiO_2 samples. As shown in Fig. 6a, the photocurrent density of photoanodes under illumination gradually increases after coupling with α-Fe_2O_3 and CdS nanoparticles, and the $CdS/Fe_2O_3/TiO_2$ NR sample exhibits the largest photocurrent density of 0.61 mA cm^{-2} at 1.2 V vs. RHE, which is almost twice of bare TiO_2 sample. I-*t* curves at a bias potential of 1.2 V vs. RHE under chopped illumination are shown in Fig. 6b, it can be seen that the samples remain excellent stability and good optical-response property under chopped illumination. $CdS/Fe_2O_3/TiO_2$ NR sample maintains a photocurrent density of about 0.6 mA cm^{-2}, which is in accordance with the LSV curves.

EIS measurement is performed under illumination and the Nyquist plots are shown in Fig. 7a and Additional file 5: Figure S4. They demonstrate that the Nyquist plots have two semicircles with a contact series resistance (R_s) on the FTO substrate. The small semicircle in the Nyquist plots is attributed to the charge transport resistance at the electrode/electrolyte interface, and the large semicircle represents the charge transfer resistance related to the electron transport/recombination within the photoanode materials. The sheet resistance (R_s) of the substrate, the charge transfer resistance of the counterelectrode (R_{ct1}), and the charge transfer resistance (R_{ct2}) were simulated by the Zview software and the corresponding data are shown in Additional file 6: Table S2. The fitted R_s and R_{ct1} values for all samples are similar due to the same configuration and growing substrates are applied, while the R_{ct2} values show obviously variation of 1079.5, 880.6, and 679.5 Ω for TiO_2, $Fe_2O_3/$

TiO_2, and $CdS/Fe_2O_3/TiO_2$, respectively. It can be seen that after modifying TiO_2 with Fe_2O_3 and CdS, the interfacial charge transfer kinetics are greatly enhanced.

The Mott-Schottky plots of the as obtained samples are listed in Fig. 7b. The slopes determined from the Mott-Schottky plots are used to estimate the carrier density according to the following equation [26]:

$$Nd = \frac{2}{e_0 \varepsilon \varepsilon_0} \times \left[\frac{dV}{d(1/C^2)} \right]$$
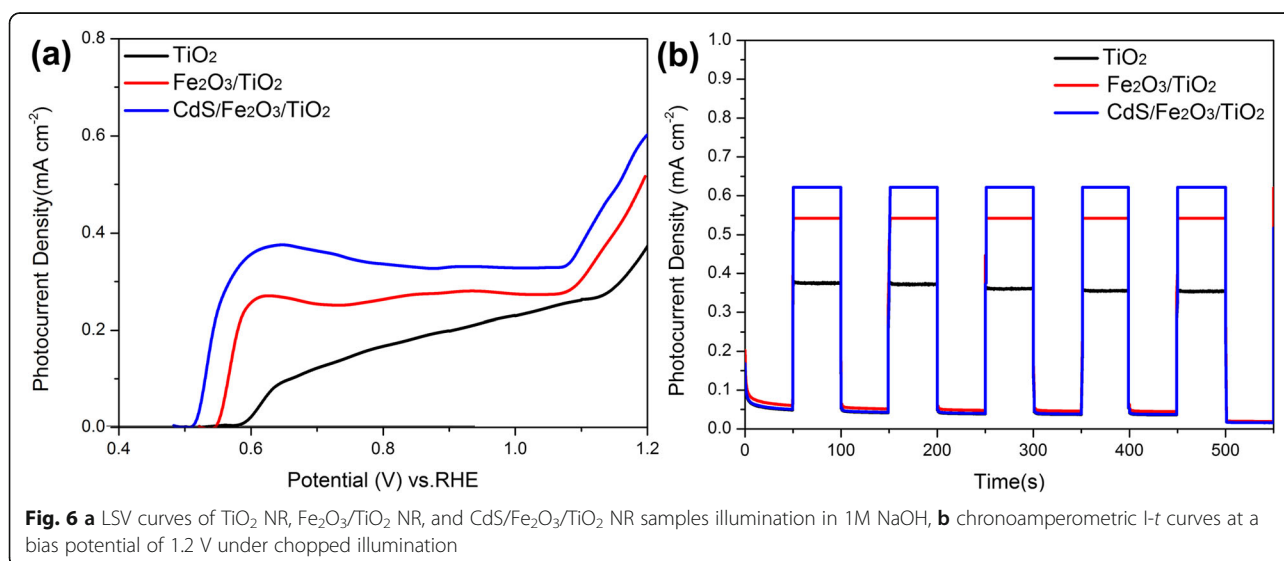
where e_0 is the electronic charge, ε is the dielectric constant of the sample, ε_0 is the permittivity of the vacuum, Nd is the donor density, and V is the applied voltage. In general, relatively smaller the slope represents higher carrier density.
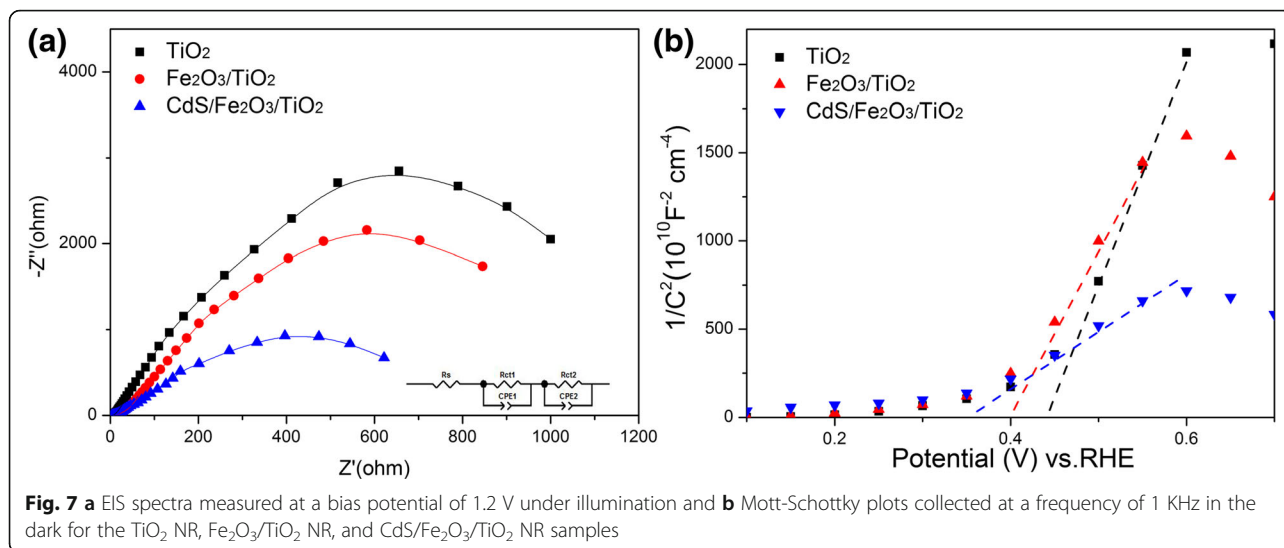
The flat band potential can be estimated by the following equation:

$$\frac{1}{C^2} = \frac{2}{e_0 \varepsilon \varepsilon_0 Nd} \times \left[E - E_{fb} - \frac{kT}{e} \right]$$

The flat band potential (E_{fb}) is determined by taking the x intercept of a linear fit to the Mott-Schottky plot, $1/C^2$, as a function of applied potential (E). Additionally, a remarkable cathodic shift in the flat potential from 0.44 V for TiO_2 sample to 0.36 V for the $CdS/Fe_2O_3/TiO_2$ NR sample was observed. This suggests a larger accumulation of electrons in the heterojunction and reflects decreased charge recombination.

It should be noticed that the PEC water oxidation performance of as synthesized CdS/ Fe2O3/TiO2 sample is comparable to some related works. For instance, Sharma et al. reported Fe-TiO_2/Zn-Fe_2O_3 thin films with a performance of 0.262 mA cm^{-2} at 0.95 V (vs. SCE) [27], while the $FTO/Fe_2O_3/ZnFe_2O_4$ photoanode achieves a photocurrent density of 0.4 mA cm^{-2} [28]. In addition,

Fig. 6 a LSV curves of TiO_2 NR, Fe_2O_3/TiO_2 NR, and $CdS/Fe_2O_3/TiO_2$ NR samples illumination in 1M NaOH, **b** chronoamperometric I-*t* curves at a bias potential of 1.2 V under chopped illumination

Yin *et al. Nanoscale Research Letters* (2017) 12:520

Page 7 of 8

Fig. 7 a EIS spectra measured at a bias potential of 1.2 V under illumination and **b** Mott-Schottky plots collected at a frequency of 1 KHz in the dark for the TiO_2 NR, Fe_2O_3/TiO_2 NR, and $CdS/Fe_2O_3/TiO_2$ NR samples

for the reported Fe_2O_3/TiO_2 nanotube photoanodes, a photocurrent density of 0.5 mA cm^{-2} is achieved [29, 30]. Comparing with the related works, it can be seen that obtained $CdS/Fe_2O_3/TiO_2$ photoanode does obtain outstanding and reliable PEC water splitting performance here.

Conclusions

In conclusion, a facile successive ionic layer adsorption and reaction (SILAR)-hydrothermal method is developed to fabricate CdS-modified Fe_2O_3/TiO_2 NR array for efficient PEC water oxidation. UV-vis study confirms the $CdS/Fe_2O_3/TiO_2$ NR array displays excellent optical response performance with an obvious broadened light absorption range. Applied as the photoanode for PEC water oxidation, $CdS/Fe_2O_3/TiO_2$ NR array photoanode exhibits greatly enhanced photocurrent density of 0.62 mA cm^{-2} (1.23 V vs. RHE) in alkaline electrolyte compared with pristine TiO_2 (0.32 mA cm^{-2} at 1.23 V vs. RHE).

Additional Files

Additional file 1: Figure S1. Cross-sectional SEM image of $CdS/Fe_2O_3/TiO_2$ NR. (JPEG 742 kb)

Additional file 2: Figure S2. The cross-view EDS mapping images of $CdS/Fe_2O_3/TiO_2$ NR in Fig. S1. (JPEG 585 kb)

Additional file 3: Figure S3. The picosecond-resolved fluorescence transients of TiO_2, Fe_2O_3/TiO_2 and $CdS/Fe_2O_3/TiO_2$ samples. (JPEG 1602 kb)

Additional file 4: Table S1. Dynamics of picosecond-resolved fluorescence transients of TiO_2, Fe_2O_3/TiO_2 and $CdS/Fe_2O_3/TiO_2$ samples. (DOCX 11 kb)

Additional file 5: Figure S4. The amplified Nyquist plot of the obtained TiO_2, Fe_2O_3/TiO_2 and $CdS/Fe_2O_3/TiO_2$ photoanodes. (JPEG 933 kb)

Additional file 6: Table S2. Series resistance of the obtained TiO_2, Fe_2O_3/TiO_2 and $CdS/Fe_2O_3/TiO_2$ photoanodes. (DOCX 13 kb)

Authors' Contributions
LWY and RT designed and supervised this work. RYY and MYL performed the simulation and wrote the manuscript. All authors read and approved the final manuscript.

Competing Interests
The authors declare that they have no competing interests.

Publisher's Note
Springer Nature remains neutral with regard to jurisdictional claims in published maps and institutional affiliations.

Author details
[1]School of Physics, Shandong University, Jinan 250100, People's Republic of China. [2]Key Laboratory for Liquid–Solid Structural Evolution and Processing of Materials, Ministry of Education, School of Materials Science and Engineering, Shandong University, Jinan 250061, People's Republic of China.

References
1. Fujishima A, Honda K (1972) Electrochemical photolysis of water at a semiconductor electrode Nature 238:37-38
2. Khan SU, Al-Shahry M, Ingler WB (2002) Efficient photochemical water splitting by a chemically modified n-TiO2 Science 297:2243-224
3. Tang R, Yin L (2015) Enhanced photovoltaic performance of dye-sensitized solar cells based on Sr-doped TiO2/SrTiO3 nanorod array heterostructures J Mater Chem A 3:17417-17425
4. Tang R, Yin R, Zhou S, Ge T, Yuan Z, Zhang L, Yin L (2017) Layered MoS2 coupled MOF-derived dual-phase TiO2 for enhanced photoelectrochemical performance J Mater Chem A 5:4962-4971
5. Resasco J, Zhang H, Kornienko N, Becknell N, Lee H, Guo J, Briseno AL, Yang P (2016) TiO2/BiVO4 nanowire heterostructure photoanodes based on type II band alignment ACS Cent Sci 2:80-88
6. Reichert R, Jusys Z, Behm R (2015) Au/TiO2 Photo (electro) catalysis: The Role of the Au Cocatalyst in Photoelectrochemical Water Splitting and Photocatalytic H2 Evolution J Phys Chem C 119:24750-24759

Yin *et al. Nanoscale Research Letters* (2017) 12:520

Page 8 of 8

7. Das RK, Kar JP, Mohapatra S (2016) Enhanced Photodegradation of Organic Pollutants by Carbon Quantum Dot (CQD) Deposited Fe3O4@mTiO2 Nano-Pom-Pom Balls Ind Eng Chem Res 55:5902-5910

8. Yang W, Yu Y, Starr MB, Yin X, Li Z, Kvit A, Wang S, Zhao P, Wang X (2015) Ferroelectric polarization-enhanced photoelectrochemical water splitting in TiO2-BaTiO3 core-shell nanowirephotoanodes Nano Lett 15:7574-7580

9. Huang B, Yang W, Wen Y, Shan B, Chen R (2014) Co3O4-modified TiO2 nanotube arrays via atomic layer deposition for improved visible-light photoelectrochemical performance ACS Appl Mater Interfaces 7:422-431

10. Hoang S, Guo S, Hahn NT, Bard AJ, Mullins CB (2011) Visible light driven photoelectrochemical water oxidation on nitrogen-modified TiO2 nanowires Nano Lett 12:26-32

11. Liu Q, Lu H, Shi Z, Wu F, Guo J, Deng K, Li L (2014) 2D ZnIn2S4 nanosheet/1D TiO2 nanorod heterostructure arrays for improved photoelectrochemical water splitting ACS Appl Mater Interfaces 6:17200-17207

12. Peerakiatkhajohn P, Yun JH, Chen H, Lyu M, Butburee T, Wang L (2016) Stable hematite nanosheet photoanodes for enhanced photoelectrochemical water splitting Adv Mater 28:6405-6410

13. Quynh LT, Van CN, Bitla Y, Chen J-W, Do TH, Tzeng W-Y, Liao S-C, Tsai K-A, Chen Y-C, Wu C-L, Lai C-H, Luo C-W, Hsu Y-J, Chu Y-H (2016) Self-Assembled BiFeO3-ε-Fe2O3 Vertical Heteroepitaxy for Visible Light Photoelectrochemistry Adv Energy Mater 6:1600686

14. Zhou S, Yin L (2017) CdS quantum dots sensitized mesoporous BiVO4 heterostructures for solar cells with enhanced photo-electrical conversion efficiency J Alloys Compd 691:040-1048

15. Bai Z, Yan X, Li Y, Kang Z, Cao S, Zhang Y (2016) 3D-Branched ZnO/CdS Nanowire Arrays for Solar Water Splitting and the Service Safety Research Adv Energy Mater 6:1501459

16. Jin-nouchi Y, Hattori T, Sumida Y, Fujishima M, Tada H (2010) PbS Quantum Dot-Sensitized Photoelectrochemical Cell for Hydrogen Production from Water under Illumination of Simulated Sunlight ChemPhysChem 11:3592–3595

17. Zhan Q, Qian J, Li X, He S (2009) A study of mesoporous silica-encapsulated gold nanorods as enhanced light scattering probes for cancer cell imaging Nanotechnol 21:055704

18. Feng X, Shankar K, Varghese OK, Paulose M, Latempa TJ, Grimes CA (2008) Verticallyaligned single crystal TiO2 nanowire arrays grown directly on transparent conducting oxide coated glass: synthesis details and applications Nano Lett 8:3781–3786

19. Cho IS, Chen Z, Forman AJ, Kim DR, Rao PM, Jaramillo TF, Zheng X (2011) Branched TiO2 nanorods for photoelectrochemical hydrogen production Nano Lett 11:4978–4984

20. Bai S, Wang L, Chen X, Du J, Xiong Y (2015) Chemically exfoliated metallic MoS2 nanosheets: A promising supporting co-catalyst for enhancing the photocatalytic performance of TiO2 nanocrystals Nano Res 8:175–183

21. Xia H, Xiong W, Lim CK, Yao Q, Wang Y, Xie J (2014) Hierarchical TiO2-B nanowire@α-Fe2O3 nanothorn core-branch arrays as superior electrodes for lithium-ion microbatteries Nano Res 7:1797–1808

22. Cao S, Yan X, Kang Z, Liang Q, Liao X, Zhang Y (2016) Band alignment engineering for improved performance and stability of ZnFe2O4 modified CdS/ZnO nanostructured photoanode for PEC water splitting Nano Energy 24:25–31

23. Yang P, Murase N (2010) Preparation-Condition Dependence of Hybrid SiO2-Coated CdTe Nanocrystals with Intense and Tunable Photoluminescence Adv Funct Mater 20:1258–1265

24. Mahadik MA, Subramanian A, Ryu J, Cho M, Jang JS (2017) A hydrothermally grown CdS nanograin-sensitized 1D Zr: α-Fe2O3/FTO photoanode for efficient solar-light-driven photoelectrochemical performance Dalton Trans 46:2377–2386

25. Zhang X, Xie Y, Chen H, Guo J, Meng A, Li C (2014) One-dimensional mesoporous Fe2O3@TiO2 core-shell nanocomposites: Rational design, synthesis and application as high-performance photocatalyst in visible and UV light region Appl Surf Sci 317:43–48

26. Kim JY, Magesh G, Youn DH, Jang J-W, Kubota J, Domen K, Lee JS (2013) Single-crystalline,wormlike hematite photoanodes for efficient solar water splitting Sci Rep 3:2681

27. Sharma P, Kumar P, Solanki A, Shrivastav R, Dass S, Satsangi VR (2012) Photoelectrochemical performance of bilayered Fe-TiO2/Zn-Fe2O3 thin films for solar generation of hydrogen J Solid State Electrochem 16:1305–1312

28. McDonald KJ, Choi K-S (2011) Synthesis and photoelectrochemical properties of Fe2O3/ZnFe2O4 composite photoanodes for use in solar water oxidation Chem Mater 23:4863–4869

29. Kuang S, Yang L, Luo S, Cai Q (2009) Fabrication, characterization and photoelectrochemical properties of Fe2O3 modified TiO2 nanotube arrays Appl Surf Sci 255:7385–7388

30. Han H, Riboni F, Karlicky F, Kment S, Goswami A, Sudhagar P, Yoo J, Wang L, Tomanec O, Petr M, Haderka O, Terashima C, Fujishima A, Schmuki P (2017) Nano 9:134–142